Tetrahedron 64 (2008) 8318–8323

Contents lists available at ScienceDirect

Tetrahedron

journal homepage: www.elsevier.com/locate/tet

A hybrid molecular machine

Valeria Amendola, Corrado Dallacosta, Luigi Fabbrizzi *, Enrico Monzani

Università di Pavia, Dipartimento di Chimica Generale, via Taramelli 12, 27100 Pavia, Italy

ARTICLE INFO

Article history:
Received 3 March 2008
Received in revised form 22 April 2008
Accepted 8 May 2008
Available online 14 May 2008

ABSTRACT

A versatile example of a molecular machine is described. The stationary part is an iron protoporphyrin complex, bearing two movable side chains with terminal donor groups. Changing the pH or the electrochemical potential, as well as the injection of CO, alters the affinity of the donor groups toward the metal ion, thus promoting intra-molecular motion of the pendant arms. The possibility of controlling the molecular motion through inputs of different nature, changeable at will, makes this system the first example of a *hybrid* molecular machine.

1. Introduction

A typical molecular machine consists of two distinct components, a mobile part and a stationary moiety, held together either by covalent bonds or by non-covalent interactions. The external operator generally regulates the displacement of the movable fragment with respect to the immovable one by means of a chemical stimulus (i.e., variation of the pH or of the redox potential) or through a physical input (i.e., light).[1] In most cases, the movement can be reversibly and repeatedly carried out, but always under the same type of input. Our aim was to develop a generation of 'hybrid' molecular machines, in which the movement could be controlled by multiple inputs, changeable at will by the operator.

Scorpionates are molecular machines consisting of a flexible pendant arm covalently bound to a stationary platform. The name 'scorpionate' comes from the similarity of the pendant arm to a scorpion tail.[2a] The stationary component is usually a macrocyclic complex, to which the mobile chain is appended. The pendant arm contains a potential donor atom, which interacts with the metal ion encircled by the macrocycle.[2b] The interaction between the pendant arm and the metal can be altered by an external input such as a variation of the pH or of the redox potential. The external impulse induces the displacement of the arm with respect to the metal containing platform, generating a controlled molecular motion. An example has been reported by our group, in which the stationary part is a Ni^{II} complex of the quadridentate macrocycle cyclam, whereas the pendant arm is a side chain containing at its end an amine nitrogen atom.[3] Altering the pH controls the position of the pendant arm, either coordinated to the Ni^{II} cation (amine form) or far away from it (ammonium form). Consecutive additions of acid and base make the pendant arm oscillate between two definite positions, thus converting the energy of a chemical process (an acid–base equilibrium) into mechanical work. As the coordination of the pendant arm modifies the electronic and the spectroscopic properties of the metal, the motion can be monitored spectrophotometrically, by recording the UV/visi spectra of the solution at different pH values. The presence of a fluorophore, such as an anthracenyl group, bound to the terminal amine group, allows the molecular movement to also be followed spectrofluorimetrically.[3a,4]

In Scheme 1 a new and versatile type of scorpionate, HM–$(GH)_2$, is shown. The stationary part is an iron protoporphyrin complex, bearing two movable side chains with terminal glycine–L-histidine–OMe groups (GH residues in the formula). In the chelated complex, the two histidine fragments occupy the axial positions of the Fe^{II} cation.

Changing the pH, as well as the injection of CO, can alter the affinity of the histidine groups toward Fe^{II}, thus promoting the detachment of one or both the pendant arms from the metal ion. The oxidation of the metal center to iron(III) induces the detachment of the bound CO and allows the coordination of the GH arm at the sixth coordination site of the iron. The possibility of controlling the molecular motion through different inputs, changeable at will, makes this system the first example of a hybrid molecular machine. Moreover, thanks to the high intensity of the hemin Soret band (i.e., around 150,000 M^{-1} cm^{-1} for the Fe(II)–CO adduct), the response is amplified and the molecular motion can be easily monitored spectrophotometrically even at very low concentrations of the complex.

2. Results and discussion

2.1. Coordinative and UV/vis spectroscopic properties of iron protoporphyrin derivatives

The UV/vis spectra of iron porphyrin derivatives show very intense bands. Generally, the intense Soret band is observed around

* Corresponding author. Tel.: +39 0382 987328.
E-mail address: luigi.fabbrizzi@unipv.it (L. Fabbrizzi).

0040-4020/$ – see front matter © 2008 Elsevier Ltd. All rights reserved.
doi:10.1016/j.tet.2008.05.041

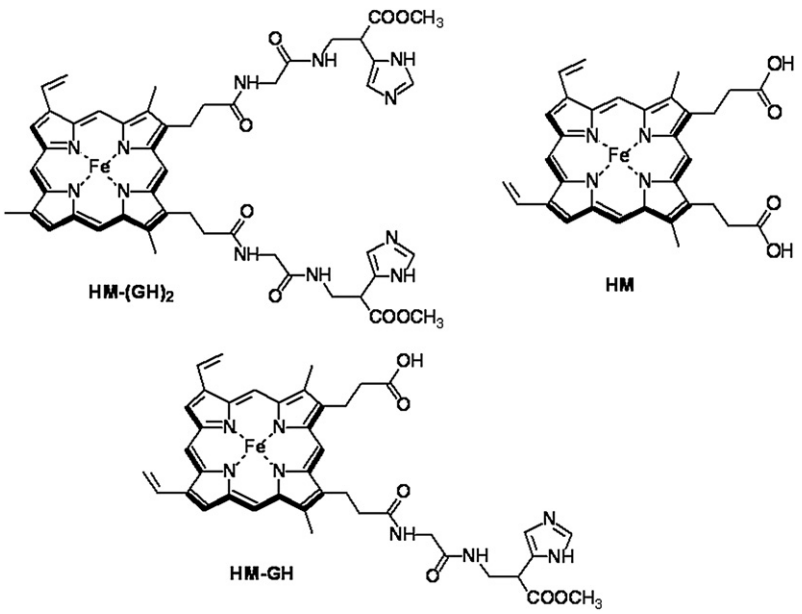

Scheme 1. Chemical structures of HM, HM–GH, and HM–$(GH)_2$.

400 nm, while the smaller β and α bands, all due to π–π transitions, are observed between 500 and 600 nm. Additionally, a ligand-to-metal charge transfer (LMCT) band occurs above 600 nm. The energy of the transitions is related to the oxidation state of the metal ion and to its spin/coordination state. For the iron(III) complexes, when the spin state of the metal ion changes from high to low, all of the bands are shifted to lower energies. On the other hand, for the iron(II) derivatives, the low-spin complexes show blue shifted bands with respect to the high-spin ones.[5]

Porphyrins and their metal complexes are known to give rise to aggregation even at micromolar concentrations. Thus, DMF was used in all the experiments performed, in order to reduce the extent of aggregation.[6] It should be noted that DMF, in the presence of a free coordination site, binds the iron center, giving rise to six-coordinated adducts. Usually the presence of a ligand at the fifth site of iron increases the binding affinity for a further ligand at the sixth site.[7] CO does not coordinate the iron(III) form of iron porphyrins, whereas it behaves as a strong ligand with iron(II) derivatives. Moreover, it exhibits a positive trans effect, thus increasing the binding affinity of the metal toward axial ligands having strong donor properties. This has been demonstrated in a variety of synthetic heme complexes.[8] The synergic bonding interaction between CO and a donor ligand facilitates the replacement of an imidazole by CO molecule from a bis-imidazole complex and, at the same time, prevents the formation of the bis CO adduct. Table 1 reports some coordinative characteristics (nature of axial ligands, spin state) and the UV/vis spectroscopic features of HM, HM–GH, and HM–$(GH)_2$ derivatives in their iron(III), iron(II), and iron(II)–CO forms.

Table 1
Spectroscopic features, spin states, and axial ligands of HM, HM–GH, and HM–$(GH)_2$ derivatives (~5 μM) in their iron(III), iron(II), and iron(II)–CO forms in DMF

Name	Complex	Oxidation state	Axial ligands	Spin state	UV/vis maxima
	HM	Iron(III)	DMF/DMF	h.s.	404, 504, 534, 626
	HM	Iron(II)	DMF/DMF	h.s.	426, 564
	HM	Iron(II)	DMF/CO	l.s.	416, 536, 568
	HM–GH	Iron(III)	His/DMF	h.s.	406, 502, 620
	HM–GH	Iron(II)	His/DMF	h.s.	430, 558
	HM–GH	Iron(II)	His/CO	l.s.	422, 540, 568
3	HM–$(GH)_2$	Iron(III)	His/His	l.s.	418, 544, 568
1	HM–$(GH)_2$	Iron(II)	His/His	l.s.	426, 530, 560
2	HM–$(GH)_2$	Iron(II)	His/CO	l.s.	420, 538, 568

2.2. Carbon monoxide induced molecular motion

The iron(II) form of the complex HM–$(GH)_2$, **1**, is in the low-spin state due to the intra-molecular coordination of two histidines from the Gly–His–OMe groups to the iron. When CO is injected with a gas-tight syringe into a solution of **1** in DMF, a change in the absorbance spectrum of the iron(II) complex is observed. A blue shift of the Soret band, from 426 to 420 nm, and a red shift of the α and β bands from 560 to 568 nm and from 530 to 538 nm, respectively, Figure 1, indicate the occurrence of CO coordination and formation of the low-spin complex **2**. The spectroscopic changes are connected with the replacement of histidine by the π-acceptor CO. Due to the high affinity of the Fe^{II} porphyrin, a CO molecule

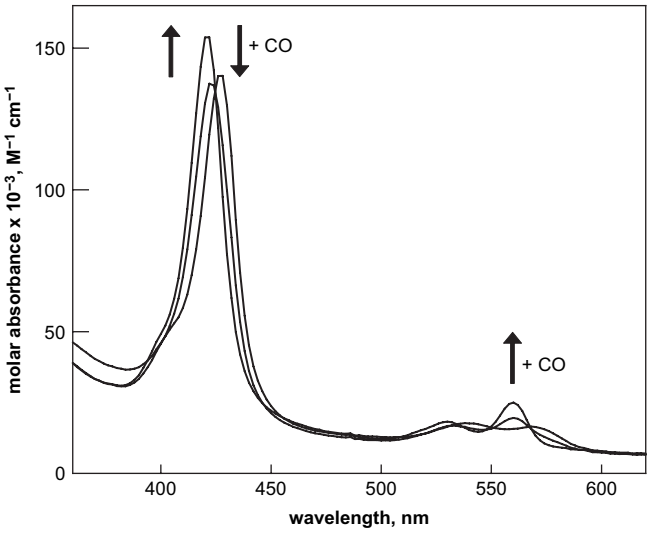

Figure 1. UV/vis spectra of the Fe(II)–CO forms of HM, HM–GH, and HM–$(GH)_2$ (~5 μM) in DMF.

replaces one of the two GH arms in complex **1**, leading to complex **2**, according to Scheme 2. The replacement of both the GH arms by CO molecules could be excluded after comparing the absorption spectrum of **2** with the ones obtained for the Fe^{II} protoheme (HM in Fig. S1) and for the monosubstituted iron(II) HM–GH complexes (Fig. S2) in the presence of CO (see Table 1). The spectroscopic features of **2** strictly resemble those of the CO adduct of the iron(II) HM–GH complex, which is known to have both a histidine and a CO bound to the iron,[9] while they are different from those obtained by bubbling CO into a heme solution in DMF (Fig. 2). The lower stability of the bis-carbonyl heme and of the CO/DMF adduct in **2** with respect to the mixed CO/Gly–His–OMe is a consequence of the strong trans effect exerted by the π-acceptor CO ligand.[5]

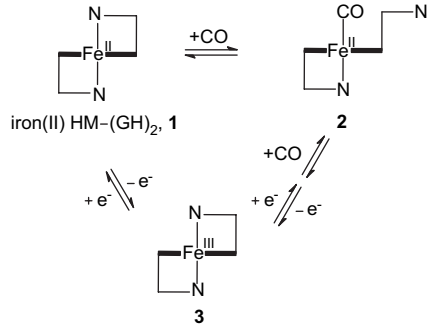

Scheme 2. Schematic representation of CO binding in HM–GH and HM–$(GH)_2$.

Purging CO by several argon/vacuum cycles (or by bubbling argon into the solution) leads to the initial bis-histidine coordinated complex. The binding/detachment of the arm to/from the Fe^{II} center is reversible and it can be followed by UV/vis spectroscopy. After gas injection, differential pulse voltammetry experiments on **1** (see Fig. 3) were carried out. The anodic shift of the peak at ca. −800 mV demonstrated the stabilizing effect exerted by CO on the low oxidation state Fe^{II}. In particular, the redox potential of the Fe^{III}/Fe^{II} couple shifts from −0.825 V versus Fc^+/Fc to −0.781 V versus Fc^+/Fc on CO coordination (ΔE=+44 mV). Moreover, the broadening of the signal, which is better appreciated in the CV experiment (Fig. 4), indicates a loss of reversibility of the Fe^{III}/Fe^{II} couple upon CO coordination.

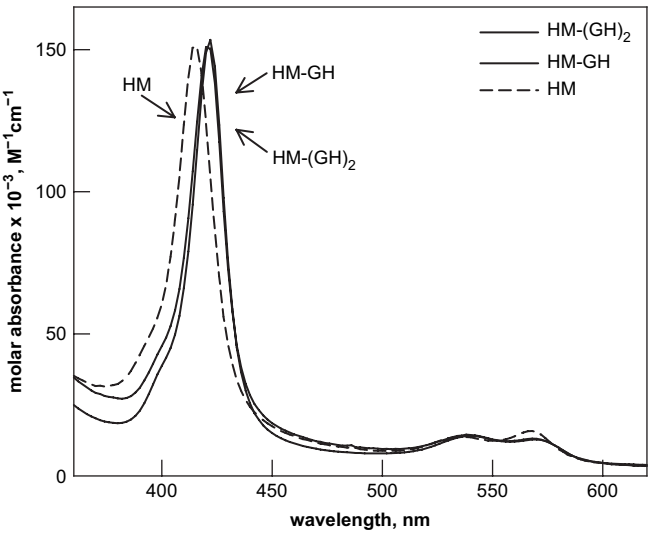

Figure 2. UV/vis spectra of the Fe(II)–CO forms of HM, HM–GH and HM–$(GH)_2$ (~5 μM) in DMF.

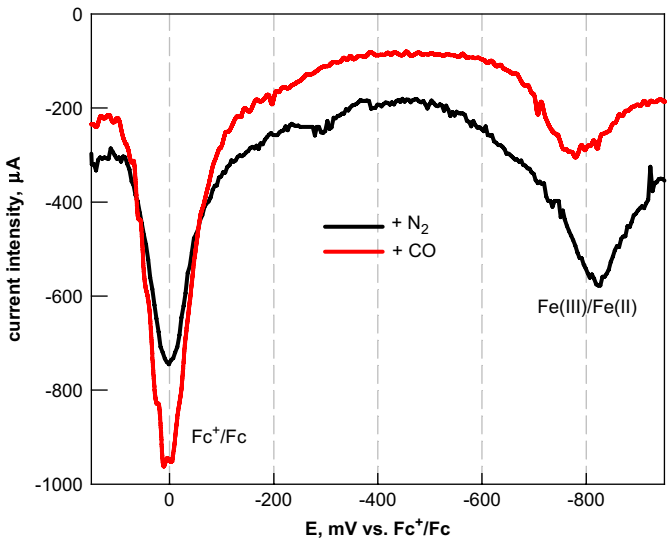

Figure 3. DPV experiment on a 5×10^{-4} M solution of the iron(II) complex of HM–$(GH)_2$, **1**, in deoxygenated DMF (black line) and in the presence of CO (red line). The Fc^+/Fc couple was used as the internal reference.

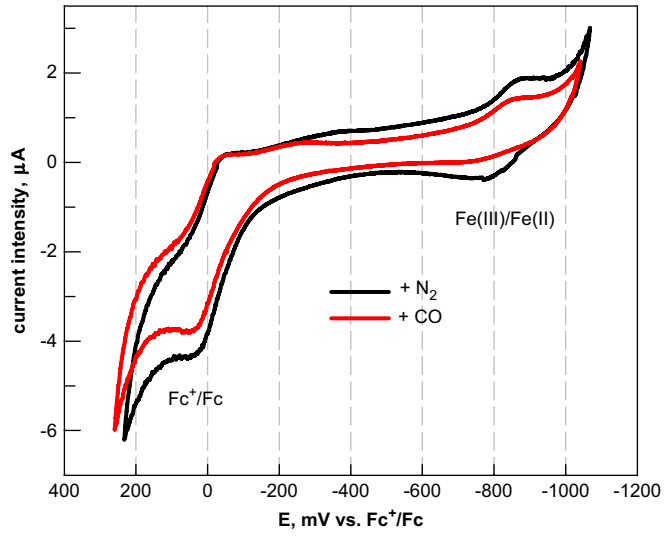

Figure 4. CV experiment on a 5×10^{-4} M solution of the iron(II) complex of HM–$(GH)_2$, **1**, in DMF. The black profile refers to the deoxygenated solution; the red line refers to the experiment conducted in the presence of CO. The Fc^+/Fc couple is the internal reference.

2.3. Gas-supported electrochemical input

Figure 5 reports the UV/vis spectra recorded over the course of a controlled potential coulometry experiment, on a deoxygenated DMF solution of **1**. The oxidation of the Fe^{II} complex (**1**) to Fe^{III} (**3**) is envisaged by the shift of the Soret band from 426 to 418 nm. After oxidation, the complex is still in low-spin state, with both the pendant arms bound to iron. If carbon monoxide is injected into a solution of the ferric complex (**3**), no displacement of the GH pendant arm is observed, due to the stronger affinity of Fe^{III} toward histidine with respect to CO.

By reversing the applied redox potential in the absence of CO, it is therefore possible to switch from the oxidized to the reduced form and vice versa, without changing the coordinative environment of the metal center. As a consequence, Fe^{III} reduction leads to the reduced species **1** and the Soret band shifts back to 426 nm. The

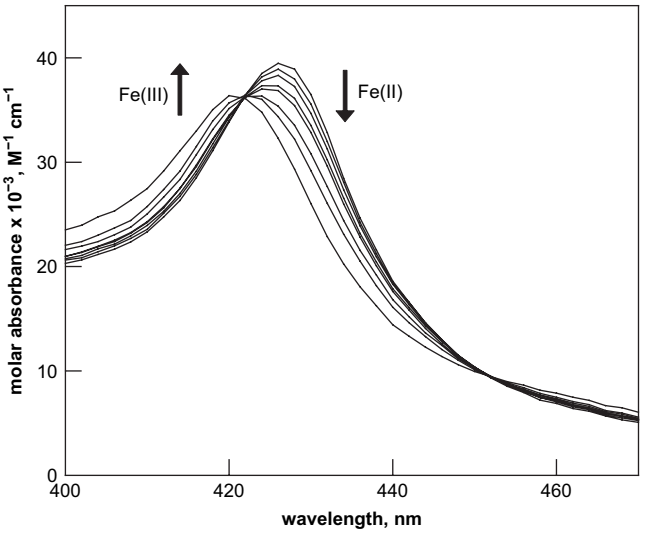

Figure 5. UV/vis spectra recorded in the course of the oxidation of the iron(II) complex of HM–$(GH)_2$, **1**, by bulk electrolysis. The experiment was performed on a 1 μM solution of **1** in deoxygenated DMF.

destabilization of the Fe^{III} form reflects the less σ-donating tendencies of CO in the axial position compared to histidine imidazole. These results are in good agreement with the reported electrochemical studies on the hemin models. On the contrary, if reduction takes place in the presence of CO, the electrochemical process is accompanied by the displacement of a GH arm by a gas molecule and complex **2** is obtained, as is demonstrated by the Soret band shift from 418 to 420 nm (see Fig. 6). At this point, starting from complex **2**, the arm folding can be achieved either by a few vacuum/argon cycles (back to complex **1**) or by Fe^{II} oxidation (leading to complex **3**). The CO-induced molecular motion involving the Fe^{II} species (**1** and **2**) is completely reversible and independent upon other stimuli (Scheme 2). On the contrary, the electrochemical input needs to be supported by the presence of the gas, in order to induce the displacement of the pendant arm from the apical position of Fe^{II}.

In conclusion, the pendant arm can be relocated at will by changing the oxidation state of the metal center. As a matter of fact, the CO-induced molecular movement of the pendant arm only takes place if the complex is in its ferrous form. Hence, the oxidation of Fe(II) to Fe(III) locks the complex in its bis-histidine coordinated form.

2.4. pH input

The presence of two histidine residues in HM–$(GH)_2$ also allows for a reversible detachment/binding of the pendant arms upon addition of acid or base to the solution of complexes **1** and **3** (as it is shown for complex **3** in Scheme 3). Figure 7 shows the spectral changes obtained upon titration of complex **3** with trifluoroacetic acid. While clear isosbestic points are not observed, one may conclude from the spectral changes that a two step protonation process takes place, eventually leading to a high-spin complex.

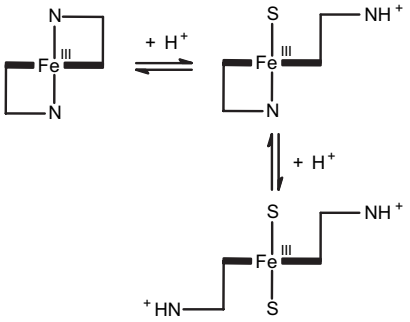

Scheme 3. Schematic representation of the protonation equilibria in HM–$(GH)_2$.

The addition of acid to complex **3** gives rise to the stepwise protonation of the coordinated histidine groups with the simultaneous detachment of the arms. After the displacement of the histidines, the axial positions of the metal center are occupied by molecules of solvent, DMF, and the complexes are high-spin. The lack of isosbestic points indicates that the two protonation steps partially overlap, probably because the release of a histidine reduces the bonding affinity of iron(III) toward the other His residue. The detachment of the arms by protonation is a reversible process: the addition of an excess of base restores the doubly GH coordinated species.

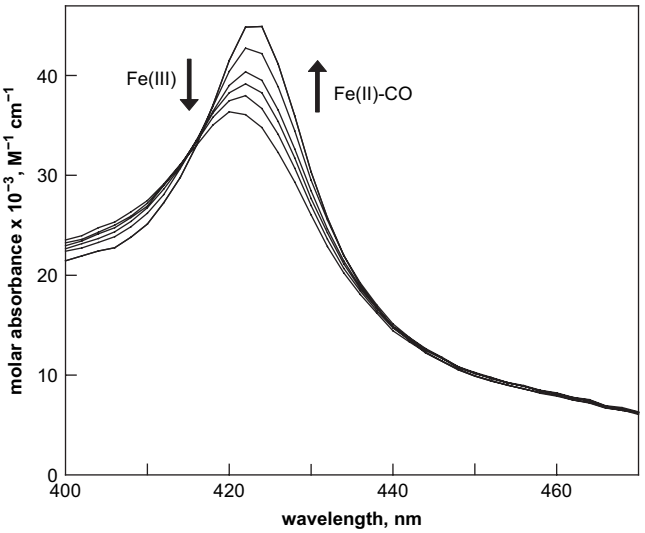

Figure 6. UV/vis spectra recorded in the course of the reduction of the iron(III) complex of HM–$(GH)_2$, **3**, by bulk electrolysis in the presence of CO. The experiment was performed on a 1 μM solution of **3**.

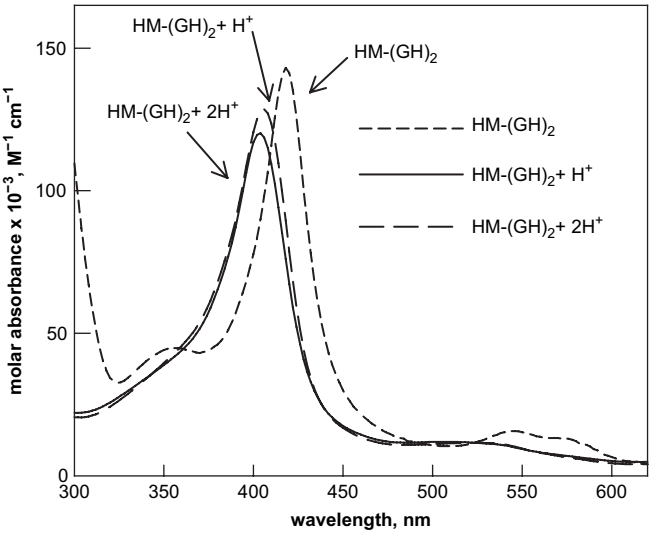

Figure 7. Spectral changes obtained upon addition of TFA to the iron(III) form of HM–$(GH)_2$ (~5 μM) in DMF.

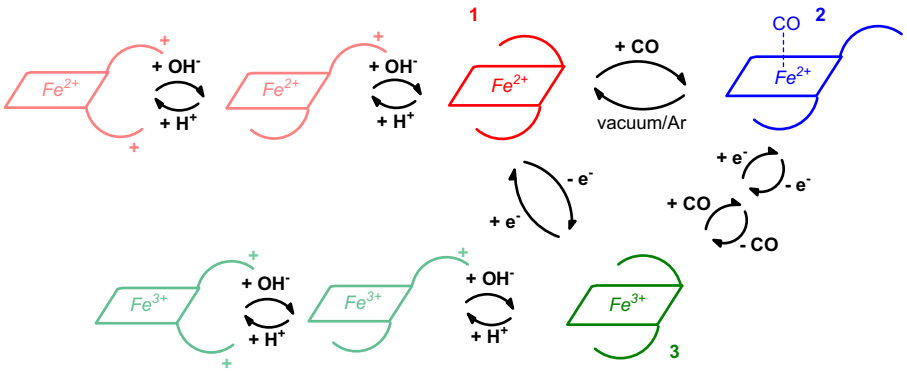

Figure 8. Dynamic effects of pH, CO/argon, and redox inputs on the movement of the GH arms in the HM–$(GH)_2$ complex.

3. Conclusion

The previously reported metal scorpionate complexes were rather simple systems providing the movement of a single movable part (a pendant arm bearing an acid–base fragment), controlled by a single input (the pH). The porphyrin based complexes reported here represent a more sophisticated version of mobile scorpionate complexes, in that: (i) they present two movable pendant arms; (ii) the motion of each pendant arm can be induced by three distinct inputs: (1) the change of the redox potential, which controls the oxidation state of the metal center, either Fe^{II} or Fe^{III}; (2) the addition of acid and base, which modifies the binding tendencies of the pendant arm, through the protonation of the histidine residue; (3) the injection of CO, which goes to occupy an axial position of the complex, thus preventing the binding of the histidine pendant arm(s). The dynamic effects of the three inputs are pictorially described in Figure 8. Motions of the pendant arm(s) can be induced by a single input or by the combination of two inputs, according to sequences of potential interest for molecular logicians.[10] At this stage, we simply call the attention on the fact that we are in presence of a molecular machine, which can be fueled by protons, electrons, and gas molecules. The change of the fuel can be done without resetting the machine, over the course of its operation. The analogy with some machines of the macroscopic world, e.g., the cars of the new generation, operating with different fuels, may justify the definition of 'hybrid molecular machines'.

4. Experimental

4.1. General

Dimethylformamide, stored over BaO, was distilled under reduced pressure over CaH_2 before use. 1-Hydroxybenzotriazole (HOBt) and H–Gly–His–OH·2HCl were obtained from Aldrich. *O*-(Benzotriazol-1-yl)-*N*,*N*,*N*′,*N*′-tetramethyluronium hexafluorophosphate (HBTU) and hemin (HM) were obtained from Fluka. CO was from SIAD. All the other reagents and solvents were of the highest grade available. HPLC runs were performed on a Jasco HPLC system equipped with two PU-1580 pumps and a MD-1510 diode array detector. UV/vis spectra were recorded on a HP8452A or a HP8453 diode array spectrophotometers.

4.2. Synthetic procedures

The syntheses of the peptide H–Gly–His–OMe and of the iron(III) complex HM–GH (Scheme 1) have been described elsewhere.[11] The synthesis of the iron(III) complex HM–$(GH)_2$ was carried out according to the following procedure. A mixture of hemin (800 mg), HOBt (1280 mg), and HBTU (930 mg) was dissolved in freshly distilled DMF (20 ml), containing triethylamine (1.6 ml). After a 10 min incubation period, H–Gly–His–OMe·2HCl (700 mg) was added and the solution was kept stirring for 10 h. The solution was dried under vacuum and the solid residue washed several times with water and diethyl ether. The crude material was purified first on a 4×40 cm silica gel column using butanol/acetic acid/water 4:1:1 (v/v/v) as eluent. The unreacted hemin eluted as the first fraction; HM–GH (as an equimolar mixture of isomeric hemins derivatized at the 6 or 7 position of the porphyrin ring) eluted as the second fraction while the bis-condensation product, HM–$(GH)_2$, remained in the column. The latter compound was then eluted by eluting with the mixture butanol/acetic acid/water 2:1:1 (v/v/v). HM–$(GH)_2$ was further purified by preparative HPLC chromatography using a SUPELCO C18 (10×25 cm) reverse phase column with a linear gradient from 0.1% TFA/water (v/v) to 0.1% TFA/CH_3CN (TFA=trifluoroacetic acid).

The iron(II) complexes were obtained by addition of the minimum amount of sodium dithionite to the deoxygenated DMF solution of the iron(III) complexes, in a cuvette fitted with a Schlenk connection. The carbon monoxide adducts were prepared by adding pure CO through a gas-tight syringe to DMF solutions of the iron(II) complexes under an argon atmosphere.

4.3. UV/vis experiments

The UV/vis spectra were recorded from 5 μM solutions of the Fe(II) and Fe(III) complexes in freshly distilled DMF. The spectra of the CO adducts were recorded after the injection of pure CO into the complex solution through a gas-tight syringe.

4.3.1. Dependence of the iron(III) HM–$(GH)_2$ complex on pH

Iron(III) HM–$(GH)_2$ was dissolved in freshly distilled DMF and diluted, until a solution with a Soret absorbance slightly below 1 was obtained. Protonation was monitored by recording the UV/vis spectra of the solution, upon the addition of small amounts of TFA 0.1 M in DMF. The acid additions caused only negligible dilutions of the solution.

4.4. Voltammetric and bulk electrolysis experiments

The DPV and CV experiments were performed in pure DMF, using a three-electrode micro cell assembly, with a nitrogen gas purging line and three platinum electrodes. The measured potential was referenced to SCE, using the Fc^+/Fc couple as the internal reference. All measurements were made on a 2×10^{-4} M solution of the complexes in DMF, at room temperature. The solution also contained Bu_4NClO_4 0.1 M as supporting electrolyte. The voltammograms were recorded from +0.2 to −0.8 V versus SCE.

The Controlled Potential Electrolysis (CPC) experiment was carried out on a MeCN solution 2×10^{-4} M in the complex and 0.1 M in $[Bu_4N]ClO_4$ by setting the potential of the working electrode

(a platinum gauze). The electrochemical oxidation/reduction of the complex was monitored by registering the UV/vis spectra of the solution over the course of the CPC experiment.

Acknowledgements

The financial support of Italian Ministry of University (PRIN—Project: Supramolecular devices) is gratefully acknowledged.

Supplementary data

In Supplementary data, the UV/vis spectra of the iron(II) and iron(II)–CO forms of HM–GH and HM are reported. Supplementary data associated with this article can be found in the online version, at doi:10.1016/j.tet.2008.05.041.

References and notes

1. Amendola, V.; Fabbrizzi, L.; Mangano, C.; Pallavicini, P. *Acc. Chem. Res.* **2001**, *34*, 488–493; Ballardini, R.; Balzani, V.; Credi, A.; Gandolfi, M. T.; Venturi, M. *Acc. Chem. Res.* **2001**, *34*, 445–455; Tian, H.; Wang, Q. C. *Chem. Soc. Rev.* **2006**, *35*, 361–374; Saha, S.; Stoddart, J. F. *Chem. Soc. Rev.* **2007**, *36*, 77–92.
2. (a) Pallavicini, P.; Perotti, A.; Seghi, B.; Fabbrizzi, L. *J. Am. Chem. Soc.* **1987**, *109*, 5139–5144; (b) Lotz, T. J.; Kaden, T. A. *Chem. Commun.* **1977**, 15–16; Lotz, T. J.; Kaden, T. A. *Helv. Chim. Acta* **1978**, *61*, 1376–1387; (c) Fabbrizzi, L.; Foti, F.; Licchelli, M.; Maccarini, P. M.; Sacchi, D.; Zema, M. *Chem. Eur. J.* **2002**, *8*, 4965–4972; (d) Boiocchi, M.; Fabbrizzi, L.; Foti, F.; Monzani, E.; Poggi, A. *Org. Lett.* **2005**, *7*, 3417–3420.
3. Fabbrizzi, L.; Licchelli, M.; Pallavicini, P.; Parodi, L. *Angew. Chem., Int. Ed.* **1998**, *37*, 800–802.
4. (a) Verdejo, B.; Ferrer, A.; Blasco, S.; Castello, C. E.; González, J.; Latorre, J.; Máñez, M. A.; Basallote, M. G.; Soriano, C.; García-España, E. *Inorg. Chem.* **2007**, *46*, 5707–5719; (b) Bencini, A.; Bianchi, A.; Lodeiro, C.; Masotti, A.; Parola, A. J.; Melo, J. S.; Pina, F.; Valtancoli, B. *Chem. Commun.* **2000**, 1639; (c) Bencini, A.; Berni, E.; Fornasari, P.; Giorgi, C.; Lima, J. C.; Lodeiro, C.; Melo, M. J.; Seixas de Melo, J. A.; Parola, A. J.; Pina, F.; Pina, J.; Valtancoli, B. *J. Chem. Soc., Dalton Trans.* **2004**, 2180–2187.
5. Owens, J. W.; O'Connor, C. J. *Coord. Chem. Rev.* **1988**, *84*, 1–45.
6. White, W. J. *The Porphyrins*; Academic: New York, NY, 1979; Vol. V, Chapter 7.
7. Yoshimura, T.; Ozaki, T. *Bull. Chem. Soc. Jpn.* **1979**, *52*, 2268–2275.
8. Jameson, G. B.; Ibers, J. A. *Comments Inorg. Chem.* **1983**, *2*, 97–126; Rougee, M.; Brault, D. *Biochemistry* **1975**, *14*, 4100–4106.
9. Gullotti, M.; Santagostini, L.; Monzani, E.; Casella, L. *Inorg. Chem.* **2007**, *46*, 8971–8975.
10. de Silva, A. P.; Gunaratne, H. Q. N.; McCoy, C. P. *Nature* **1993**, *364*, 42–44; de Silva, A. P.; Gunaratne, H. Q. N.; McCoy, C. P. *J. Am. Chem. Soc.* **1997**, *119*, 7891–7892; de Silva, A. P.; Dixon, I. M.; Gunaratne, H. Q. N.; Gunnlaugsson, T.; Maxwell, P. R. S.; Rice, T. E. *J. Am. Chem. Soc.* **1999**, *121*, 1393–1394; de Silva, A. P.; McClenaghan, N. D. *J. Am. Chem. Soc.* **2000**, *122*, 3965–3966; de Silva, A. P. *Nat. Mater.* **2005**, *4*, 15–16; de Silva, A. P.; Uchiyama, S. *Nat. Nanotechnol.* **2007**, *27*, 399–410.
11. (a) De Sanctis, G.; Fasciglione, G. F.; Marini, S.; Sinibaldi, F.; Santucci, R.; Monzani, E.; Dallacosta, C.; Casella, L.; Coletta, M. *J. Biol. Inorg. Chem.* **2006**, *11*, 153–167; (b) Roncone, R.; Monzani, E.; Murtas, M.; Battaini, G.; Pennati, A.; Sanangelantoni, A. M.; Zuccotti, S.; Bolognesi, M.; Casella, L. *Biochem. J.* **2004**, *377*, 717–724; (c) Ryabova, E. S.; Dikiy, A.; Hesslein, A. E.; Bjerrum, M. J.; Ciurli, S.; Nordlander, E. *J. Biol. Inorg. Chem.* **2004**, *9*, 385–395.